

## Supporting Information

### Stable and Efficient Organic Solar Cells Featuring an Ultra-thin and Transparent Solution-Deposited MoO<sub>3</sub> Hole Extraction Layer

*Wisnu Tanyo Hadmojo,<sup>\*ab</sup> Hendrik Faber,<sup>a</sup> Julien Gorenflot,<sup>a</sup> Ryanda Enggar Anugrah Ardhi,<sup>a</sup> Zhaoheng Ling,<sup>a</sup> Qiao He,<sup>c</sup> Sarah Fearn,<sup>c</sup> Ayman Rezk,<sup>b</sup> Muntaser Almansoori,<sup>d</sup> Ammar Nayfeh,<sup>b</sup> Martin Heeney,<sup>a</sup> Frédéric Laquai,<sup>a</sup> and Thomas D. Anthopoulos<sup>\*ae</sup>*

<sup>a</sup> KAUST Solar Center (KSC), Physical Sciences and Engineering Division (PSE), King Abdullah University of Science and Technology (KAUST), Thuwal, 23955-6900, Kingdom of Saudi Arabia

<sup>b</sup> Department of Electrical Engineering, Khalifa University, United Arab Emirates

<sup>c</sup> Department of Chemistry and Centre for Processable Electronics, Imperial College London, London W12 0BZ, UK

<sup>d</sup> Department of Mechanical & Nuclear Engineering, Khalifa University, United Arab Emirates

<sup>e</sup> Henry Royce Institute and Photon Science Institute, Department of Electrical and Electronic Engineering, The University of Manchester, Oxford Road, Manchester M13 9PL, United Kingdom

#### AUTHOR INFORMATION

#### Corresponding Authors

\*Email: [thomas.anthopoulos@manchester.ac.uk](mailto:thomas.anthopoulos@manchester.ac.uk); [wisnu.hadmojo@ku.ac.ae](mailto:wisnu.hadmojo@ku.ac.ae)

## Experimental details

*Materials:* PM6: (Poly[(2,6-(4,8-bis(5-(2-ethylhexyl-3-fluoro)thiophen-2-yl)-benzo[1,2-b:4,5-b']dithiophene))-alt-(5,5-(1',3'-di-2-thienyl-5',7'-bis(2-ethylhexyl)benzo[1',2'-c:4',5'-c']dithiophene-4,8-dione)]), and L8-BO: (2,2'-((2Z,2'Z)-((12,13-bis(2-ethylhexyl)-3,9-(2-butyloctyl)-12,13-dihydro-[1,2,5]thiadiazolo[3,4-e]thieno[2'',3''':4',5']thieno[2',3':4,5]pyrrolo[3,2-g]thieno[2',3':4,5]thieno[3,2-b]indole-2,10-diyl)bis(methanylylidene))bis(5,6-difluoro-3-oxo-2,3-dihydro-1H-indene-2,1-diylidene))dimalononitrile). PM6 and L8-BO were purchased from Solarmer and Derthon, respectively. ZnO (Zinc oxide nanoparticle) was purchased from avantama. 2PACz ((2-(9H-carbazol-9-yl)ethyl)phosphonic acid) ([2-(3,6-Dimethoxy-9H-carbazol-9-yl)ethyl]phosphonic Acid) and s-MoO<sub>x</sub> (Ammonium molybdate (para) tetrahydrate, 99%) were purchased from TCI chemical and Sigma, respectively. PEDOT:PSS (4083) and e-MoO<sub>x</sub> (Molybdenum (VI) oxide trace metals, 99.97%) were purchased from Heraeus and Sigma, respectively.

*Solar Cell Fabrication:* The ITO substrates were pre-cleaned by soaking in ultrasonication bath using detergent, deionized water, acetone, and IPA, respectively, for 10 min. Then, ITO substrates were treated by UV-ozone treatment for 20 min. Solution for 2PACz and s-MoO<sub>x</sub> were prepared and deposited in air. The precursor of 2PACz and s-MoO<sub>x</sub> were dissolved using absolute ethanol (0.5 mg/ml) and deionized water (5 mg/ml), respectively. 2PACz (~3 nm) was deposited by spin coating at 5000 rpm, followed by thermal annealing at 80 °C for 1 min. s-MoO<sub>x</sub> (< 5 nm) was deposited by spin coating at 5000 rpm, followed by thermal annealing at 150 °C for 30 min. Then, the substrates were transferred into N<sub>2</sub> based glove box for active layer deposition. Blend PM6:L8-BO (17.6 mg/ml in Chloroform w/ 0.5% DIO) were stirred at 40 °C for 1 h in the glove box. The active layer were spin coated on the substrates at ~3500 rpm (~110 nm). Next, ZnO (20 nm) was spin-coated onto the substrates, followed by thermal annealing at 80 °C for 1 min. Finally, Ag (150

nm) was deposited by thermal evaporation and under reduced pressure ( $< 4 \times 10^{-6}$  Pa). The active area of OSCs is  $0.1 \text{ cm}^2$ .

*Device characterization:* UV-vis measurement were performed using Cary 5000 spectrophotometer. IE measurements were carried out using photoelectron spectroscopy in air (PESA).  $J$ - $V$  curves were obtained by using Keithley 2400 source meter and Oriel Class AAA solar simulator calibrated to 1 sun using silicon reference from Newport. EQE spectra were measured using solar cell spectral response measurement system QE-R3011 (Enli tech.). Both  $J$ - $V$  and EQE were performed inside  $\text{N}_2$  glove box. Operational stability tests were performed under low humidity chamber and the samples were illuminated with white light (Thorlabs, MCWHL5) and tracking the maximum power point condition. Cells that underwent the thermal and operational stability tests were not encapsulated. Hole-only devices for SCLC measurements were conducted under dark inside  $\text{N}_2$  glove box. The hole and electron mobilities were determined by fitting the dark current using the following equation:

$$J = \frac{9}{8} \varepsilon_0 \varepsilon_r \mu \frac{V^2}{d^3} \quad (\text{Eq. SI-1})$$

$J$  is the dark current.  $\varepsilon_0$  and  $\varepsilon_r$  are permittivity of vacuum and relative permittivity of materials, respectively.  $V$  is the effective voltage and  $d$  is the thickness of active materials. The mobility is calculated from the slope of  $J^{1/2}$ - $V$ .

Photo electron spectroscopy in air (PESA) (Riken AC-2, Hitachi) was utilized to measure IE of materials. XPS measurements were performed using an Omicron spectrometer with a monochromatic Al  $K\alpha$  X-Ray Omicron XM1000 X-ray source (1486.6 eV) at reduced pressure ( $10^{-9}$ ). AFM images were obtained using Bruker in tapping mode. Transient photo-voltage (TPV) measurements were carried out using PAIOS. Small optical perturbation was applied ( $< 3\%$  of the

$V_{OC}$ ), and the voltage decay was observed to monitor the bimolecular charge carrier recombination.

The charge carrier lifetime was determined by the voltage decay equation:

$$V(t) = V_{OC} + \Delta V \exp(-t/\tau) \quad (\text{Eq. SI-2})$$

$\Delta V$  is the voltage difference due to the laser pulse,  $t$  is the time, and  $\tau$  is the charge carrier lifetime.

Transient photo-current (TPC) measurements were carried out using PAIOS. The cells were excited using a square shaped light pulse with different intensity (5-200 mW/cm<sup>2</sup>) for 200  $\mu$ s. EIS measurements were conducted under dark and frequency between 300 Hz to 3 MHz using PAIOS. The values obtained from Nyquist plot were simulated based on the equivalent circuit and extracted using Zview software (Scribner Associates) using a non-linear least square methods.  $R_{\text{electrodes}}$  is the total resistance of all electrodes.  $R_{\text{interfaces}}$  is the total resistance of all the interfaces.  $R_{\text{BHJ}}$  is the total resistance only in BHJ films. Constant phase element (CPE) describe the capacitive behaviour of non-ideal capacitors, while CPE-T and CPE-P is the specific pseudo-capacitance and inhomogenous capacitive constant, respectively.

Depth profiles of the samples were carried out using an IONTOF ToF-SIMS V instrument in non-interlaced mode. A 25 KeV Bi<sup>3+</sup> ion beam was used to analyse the samples over an area of 100 mm<sup>2</sup>. Depth profiling was carried out using a 500eV Cs<sup>+</sup> ion beam, with a current of 40 nA, over an area of 400mm<sup>2</sup>. Negative secondary ions were collected.

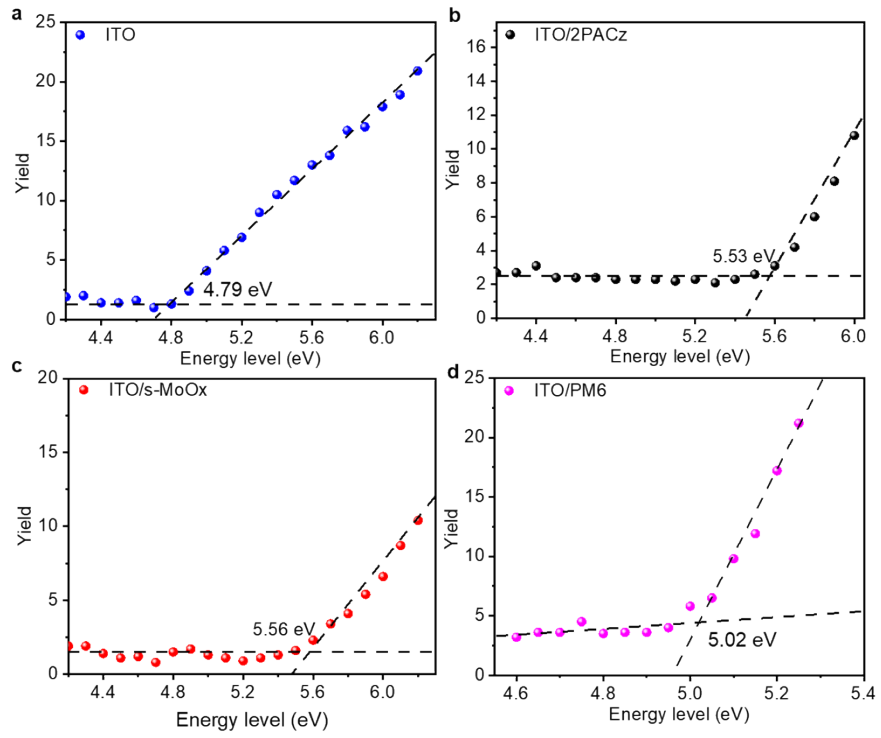


**Figure S1.** IE of (a) ITO, (b) ITO/2PACz, (c) ITO/s-MoO<sub>x</sub>, and (d) ITO/PM6.

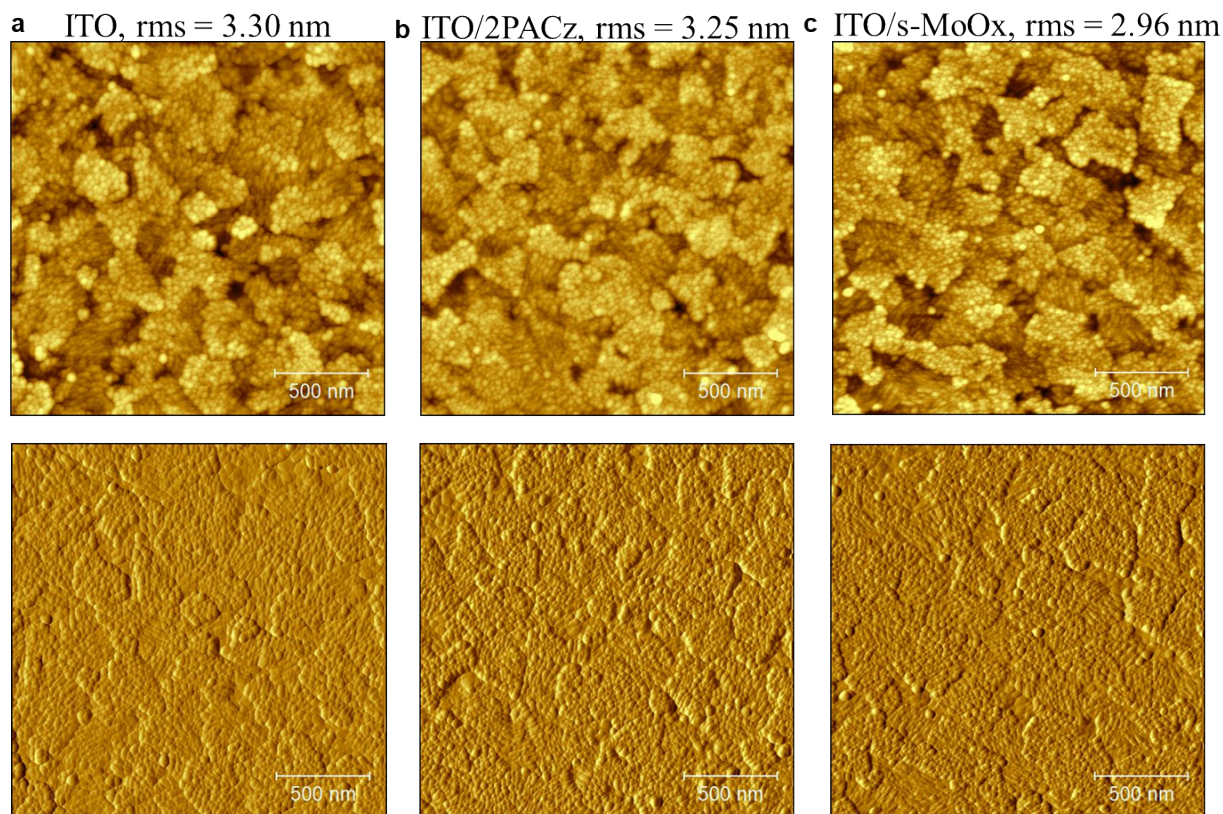


**Figure S2.** AFM height (above) and phase (bottom) images of (a) ITO, (b) ITO/2PACz, and (c) ITO/s-MoO<sub>x</sub>.

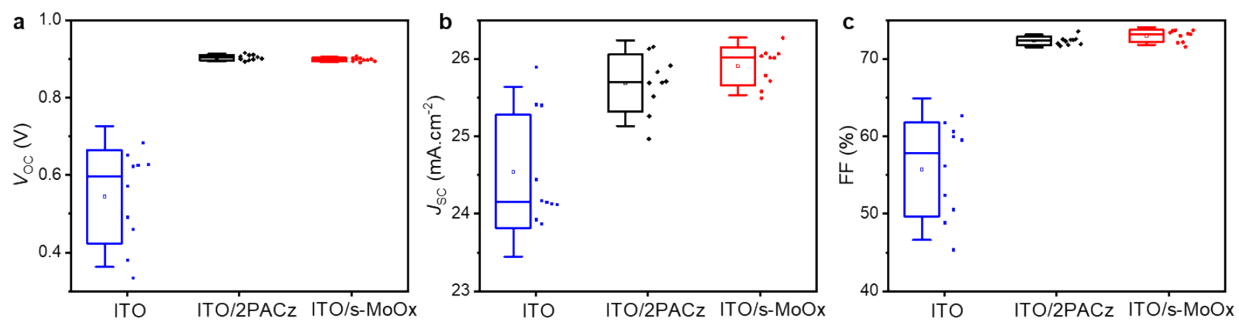


**Figure S3.** Statistics of (a)  $V_{OC}$ , (b)  $J_{SC}$ , and (c) FF of 10 cells incorporating PM6:L8-BO BHJ system with ITO, ITO/2PACz, and ITO/s-MoO<sub>x</sub> as HELs.

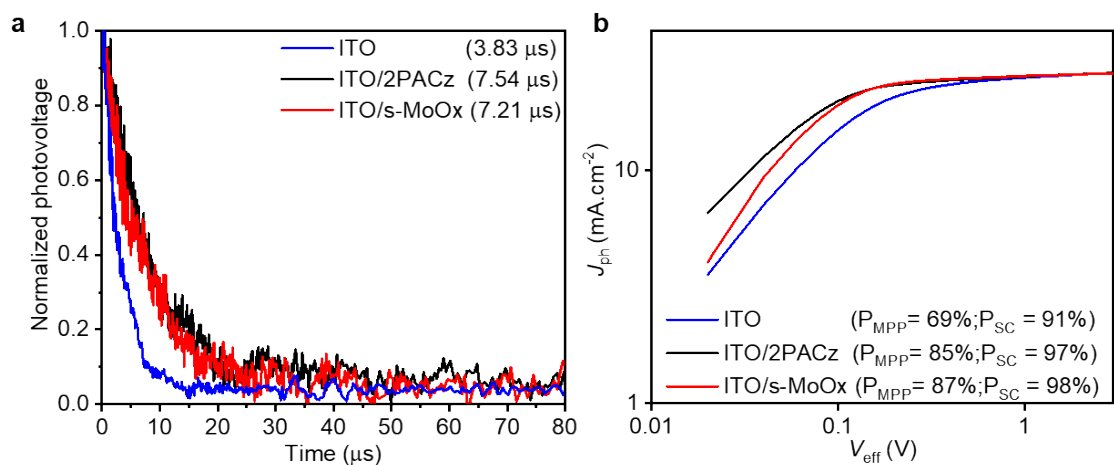


**Figure S4.** a) TPV and b)  $V_{\text{eff}}$  vs  $J_{\text{ph}}$  measurements of cells incorporating PM6:L8-BO BHJ system with ITO, ITO/2PACz, and ITO/s-MoO<sub>x</sub> as HELs.

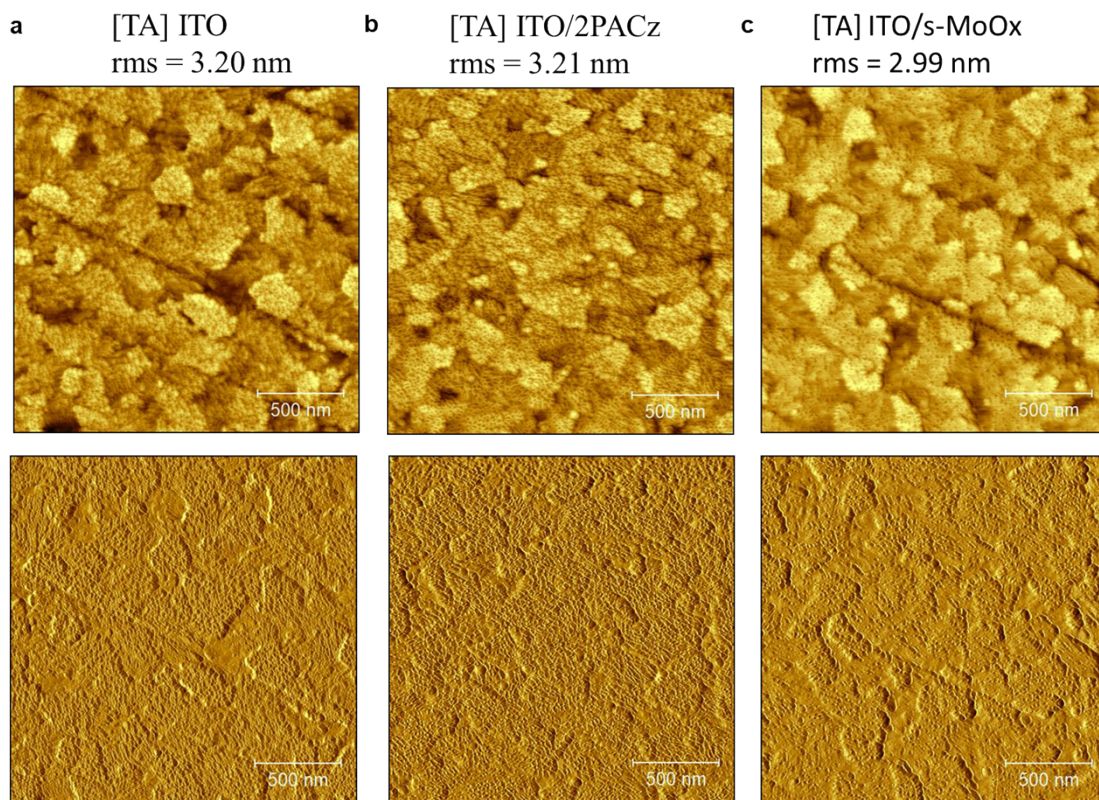


**Figure S5.** AFM height (above) and phase (bottom) images of (a) ITO, (b) ITO/2PACz, and (c) ITO/s-MoO<sub>x</sub> after thermal annealed at 85 °C for 200 h.

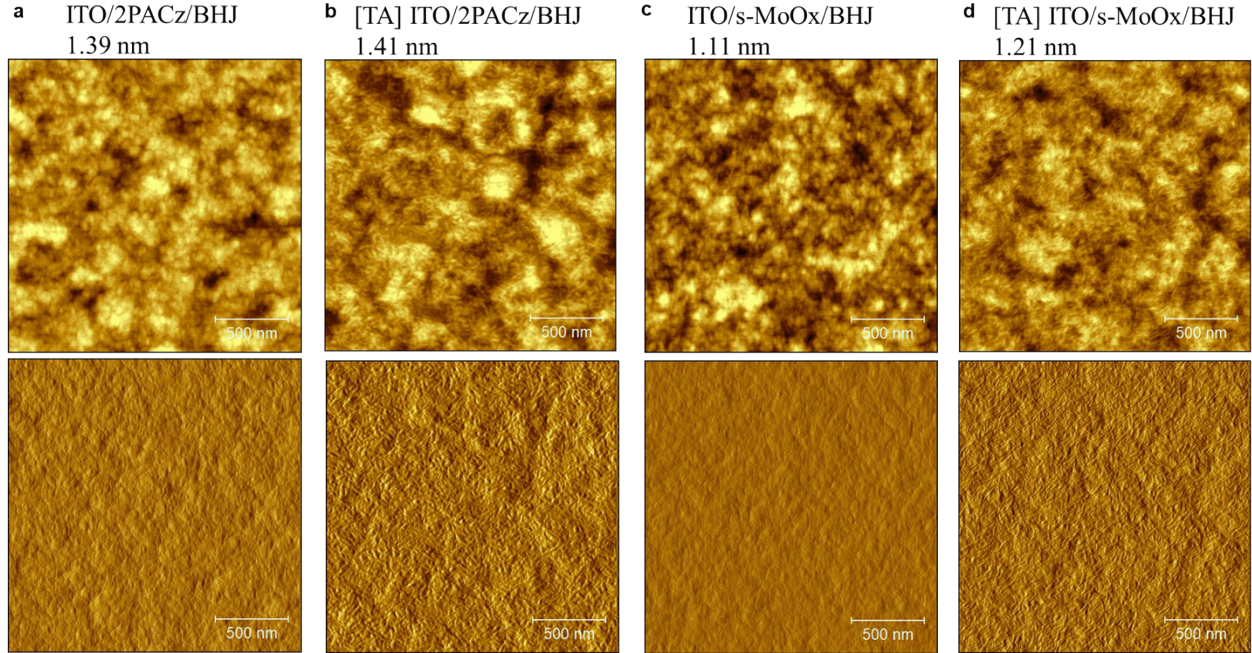


**Figure S6.** AFM height (above) and phase (bottom) images of fresh and thermal annealed [TA] at 85 °C for 200 h of half-full cells based on (a) ITO/2PACz/BHJ, (b) [TA] ITO/2PACz/BHJ, (c) ITO/s-MoO<sub>x</sub>/BHJ, and (d) [TA] ITO/s-MoO<sub>x</sub>/BHJ.

**Table S1.** Summary of the hole mobility values of the PM6:L8-BO devices featuring different HELs before and after thermal stress at 85 °C for 200 h.

ITO/HEL/PM6:L8-BO/Au	Hole mobility ( $\times 10^{-4}$ ) (cm <sup>2</sup> V <sup>-1</sup> s <sup>-1</sup> )		
	Fresh	TA 85 °C	TA/Fresh
No HEL	0.06	0.00003	0.0005
2PACz	1.30	0.10	0.08
s-MoO <sub>x</sub>	1.32	1.22	0.92

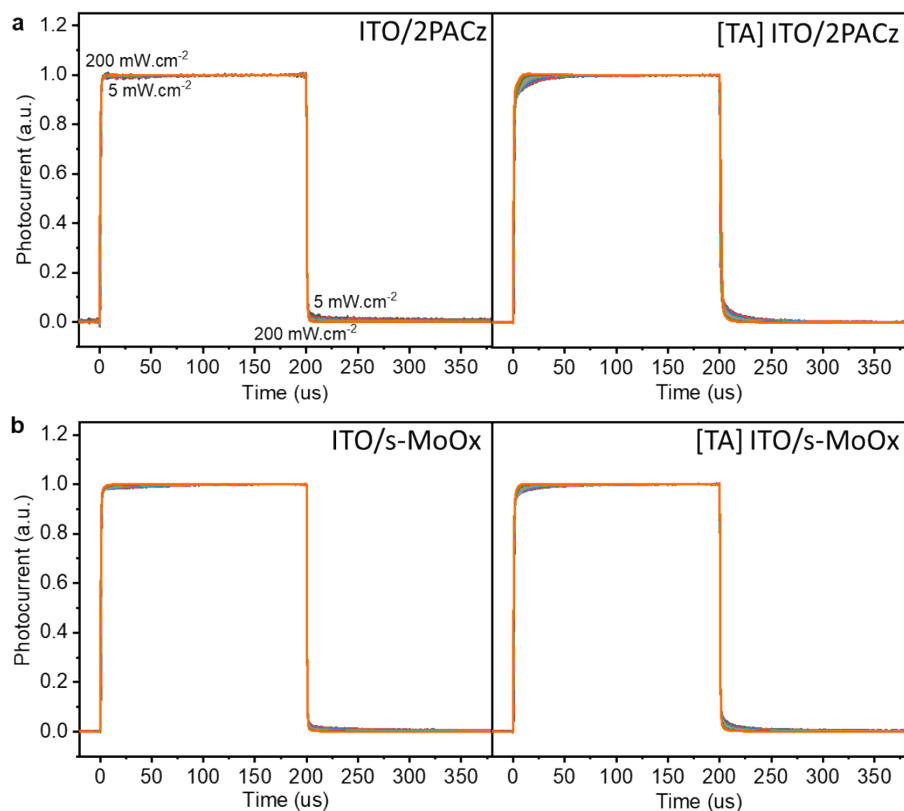


**Figure S7.** TPC spectra of fresh (left) and thermal annealed [TA] at 85 °C for 200 h (right) of OSCs based on (a) ITO/2PACz/BHJ/ZnO/Ag and (b) ITO/s-MoO<sub>x</sub>/BHJ/ZnO/Ag.

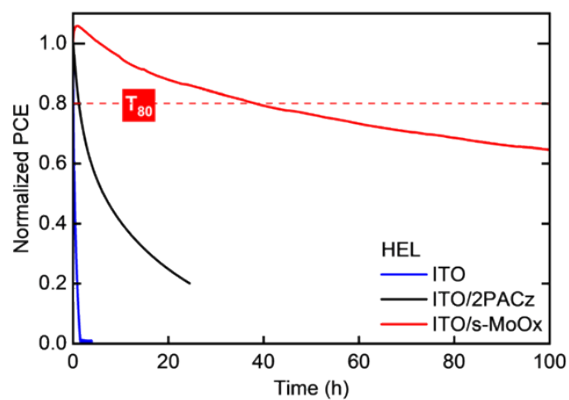


**Figure S8.** Operational stability (LED illumination with MPPT) performed on PM6:L8-BO featuring ITO, ITO/2PACz, and ITO/s-MoO<sub>x</sub> as HELs. The measurement were performed under low humidity chamber filled with N<sub>2</sub>.

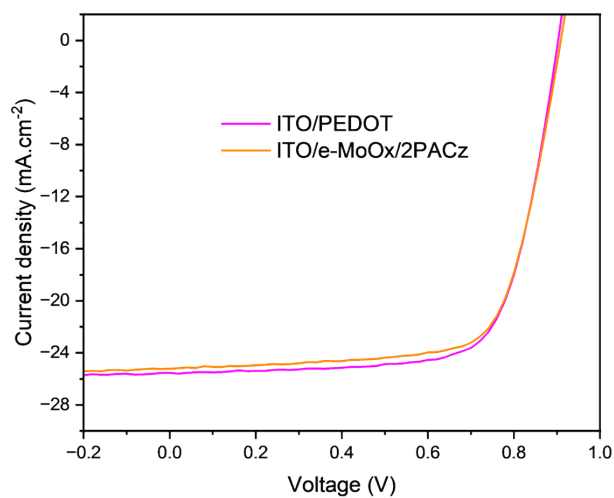


**Figure S9.**  $J$ - $V$  curve of PM6:L8-BO OSCs featuring ITO/PEDOT:PSS and ITO/e-MoO<sub>x</sub>/2PACz as HTL.

**Table S2.** Best solar cell parameters measured for PM6:L8-BO OSCs featuring PEDOT:PSS and e-MoO<sub>x</sub>/2PACz as HTL. The statistics were derived from measurements obtained for 10 devices.

HTL	PCE (%)	$V_{oc}$ (V)	$J_{sc}$ (mA/cm <sup>2</sup> )	FF (%)
PEDOT:PSS	16.65 (16.39 ± 0.18)	0.90 (0.90 ± 0.01)	25.53 (25.16 ± 0.47)	72.26 (72.70 ± 1.01)
e-MoO <sub>x</sub> /2PACz	16.42 (16.33 ± 0.08)	0.91 (0.90 ± 0.01)	25.22 (25.56 ± 0.55)	71.66 (71.28 ± 1.24)

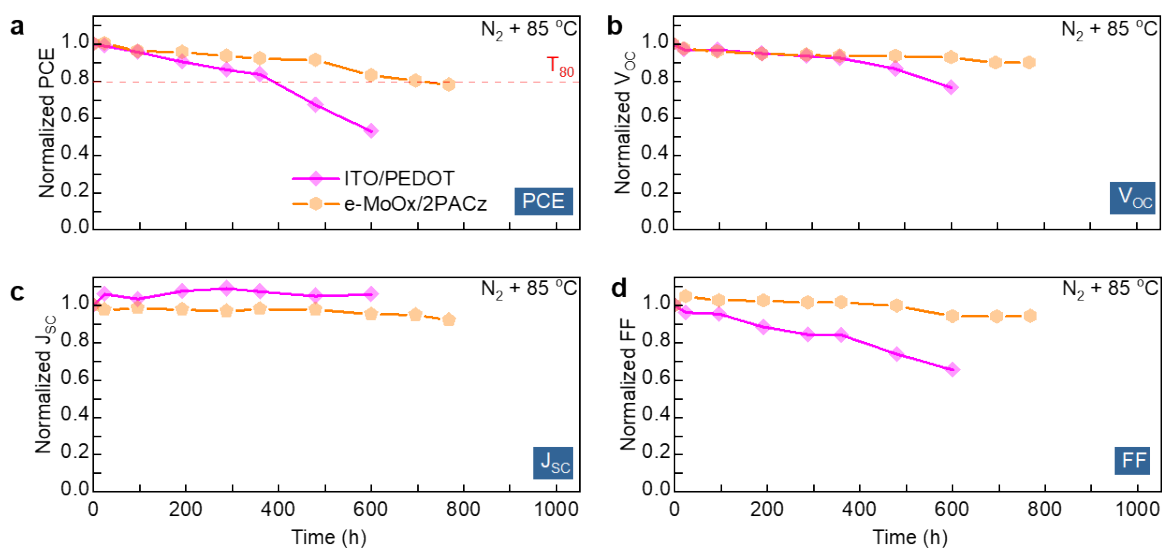


**Figure S10.** Evolution of cells parameters including (a) PCE, (b)  $V_{OC}$ , (c)  $J_{SC}$ , and (d) FF featuring PM6:L8-BO as active materials and PEDOT:PSS or e-MoO<sub>x</sub>/2PACz as HTL. Cells were stored under a dark and  $N_2$  atmosphere while continuously annealed at  $85^\circ C$ .

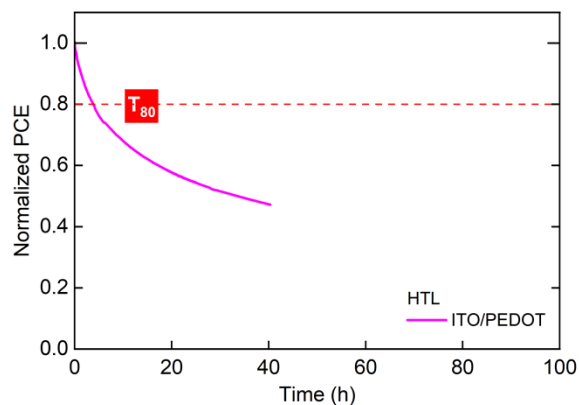


**Figure S11.** Operational stability performed on PM6:L8-BO featuring PEDOT:PSS as HTL. The measurement were performed under low humidity chamber filled with  $N_2$ .

**Table S3.** Summary of OSCs parameters and stability featuring various SAM as HELs.

Active Materials	HEL	$V_{OC}$ (V)	$J_{SC}$ (mA.cm <sup>-2</sup> )	FF (%)	PCE (%)	$T_{80}$	Year
PM6:L8-BO	s-MoO <sub>x</sub>	0.90	26.07	73.6	17.27	600 h (85 °C) 37 h (light)	<b>This work</b>
PM6:L8-BO	2PACz	0.90	26.16	73.6	17.26	15 h (85 °C) 1.2 h (light)	<b>This work</b>
PM6:PJ1- $\gamma$	2PACz	0.94	26.67	76.4	19.19	48 h (light)	2025 <sup>[1]</sup>
PM6:BTP-eC9:dT9TBO	JJ26	0.92	27.47	77.0	19.35	710 h (light)	2025 <sup>[2]</sup>
PM6:L8-BO :BTP-eC9	3-BPIC-F	0.87	28.12	80.4	19.71	700 h (65 °C)	2024 <sup>[3]</sup>
PM6:BTP-eC9	4PADBT :HOBT	0.86	28.69	79.3	19.66	5 h (65 °C) 200 h (light)	2024 <sup>[4]</sup>
PM6:PTQ10 :m-BTP-phC6	2PACz :PyCA-3F	0.88	27.57	80.8	19.51	1000 h (light)	2024 <sup>[5]</sup>
PM6:BTP-eC9 :L8-F	Br-2PACz :HPWO	0.87	28.20	77.5	19.10	1000 h (light)	2024 <sup>[6]</sup>
D18:Y6	Cl-I-2	0.85	27.30	77.5	18.10	N/A	2024 <sup>[7]</sup>
PM6:BTP-eC9 :L8-BO-F	4,5-Cl- 2PACz	0.86	28.56	77.8	19.00	800 h (light)	2023 <sup>[8]</sup>
PM6:BTP-eC9	DCB-BPA	0.86	28.07	75.2	18.20	30 h (light)	2023 <sup>[9]</sup>
PM6:BO-4Cl	BNPA /F5BNPA	0.84	28.70	74.4	18.00	10 h (light)	2023 <sup>[10]</sup>
PM6:BTP-eC11	Br-2EPSe	0.85	27.87	75.1	17.90	N/A	2022 <sup>[11]</sup>
PM6:BTP-eC9	3PACz	0.86	25.30	78.0	17.40	N/A	2022 <sup>[12]</sup>
P3HT:PCBM	FSAM	0.58	8.75	52.0	2.61	N/A	2013 <sup>[13]</sup>
P3HT:PCBM	CF3 SAM	0.60	13.87	38.0	3.15	N/A	2007 <sup>[14]</sup>

**References**

- [1] H. Huang, G. Zhang, C. Xie, Z. Li, Q. Bai, B. He, M. Qiu, P. Han, H. Hu, S. Li, G. Zhang, *Adv Funct Mater* **2025**, 35.
- [2] W. Jiang, Y. Li, H. Gao, L. Kong, C. Wong, X. Yang, F. R. Lin, A. K. -Y. Jen, *Angewandte Chemie International Edition* **2025**.
- [3] H. Liu, Y. Xin, Z. Suo, L. Yang, Y. Zou, X. Cao, Z. Hu, B. Kan, X. Wan, Y. Liu, Y. Chen, *J Am Chem Soc* **2024**, 146, 14287.
- [4] X. Sun, X. Ding, F. Wang, J. Lv, C. Gao, G. Zhang, X. Ouyang, G. Li, H. Hu, *ACS Energy Lett* **2024**, 9, 4209.
- [5] D. Li, Q. Lian, T. Du, R. Ma, H. Liu, Q. Liang, Y. Han, G. Mi, O. Peng, G. Zhang, W. Peng, B. Xu, X. Lu, K. Liu, J. Yin, Z. Ren, G. Li, C. Cheng, *Nat Commun* **2024**, 15, 7605.
- [6] B. Fan, H. Gao, Y. Li, Y. Wang, C. Zhao, F. R. Lin, A. K.-Y. Jen, *Joule* **2024**, 8, 1443.
- [7] M. Li, Z. Li, H. Fu, R. Yu, W. Jiang, F. Qi, F. R. Lin, G. Chen, A. Walsh, A. K.-Y. Jen, *ACS Appl Energy Mater* **2024**, 7, 1306.
- [8] Y. Wang, W. Jiang, S. Liu, C. Lin, B. Fan, Y. Li, H. Gao, M. Liu, F. R. Lin, A. K. -Y. Jen, *Adv Energy Mater* **2024**, 14.
- [9] W. Wang, Z. Lin, S. Gao, W. Zhu, X. Song, W. Tang, *Adv Funct Mater* **2023**, 33.
- [10] J. Hu, C. He, X. Zheng, Y. Li, X. Yang, W. Wang, J. Zhang, Q. Chen, F. Huang, W. Fu, H. Chen, *Solar RRL* **2023**, 7.
- [11] A. Ullah, K. H. Park, Y. Lee, S. Park, A. Bin Faheem, H. D. Nguyen, Y. Siddique, K. Lee, Y. Jo, C. Han, S. Ahn, I. Jeong, S. Cho, B. Kim, Y. S. Park, S. Hong, *Adv Funct Mater* **2022**, 32.
- [12] H. Bin, K. Datta, J. Wang, T. P. A. van der Pol, J. Li, M. M. Wienk, R. A. J. Janssen, *ACS Appl Mater Interfaces* **2022**, 14, 16497.
- [13] H. Wang, E. D. Gomez, Z. Guan, C. Jaye, M. F. Toney, D. A. Fischer, A. Kahn, Y.-L. Loo, *The Journal of Physical Chemistry C* **2013**, 117, 20474.
- [14] J. S. Kim, J. H. Park, J. H. Lee, J. Jo, D.-Y. Kim, K. Cho, *Appl Phys Lett* **2007**, 91.